Int. J. Heat Mass Transfer. Vol. 32, No. 9, pp. 1779–1787, 1989
Printed in Great Britain

0017–9310/89 $3.00 + 0.00
© 1989 Pergamon Press plc

Combined heat and mass transfer natural convection between vertical parallel plates

D. J. NELSON
Department of Mechanical Engineering, Virginia Polytechnic Institute and State University, Blacksburg, VA 24061, U.S.A.

and

B. D. WOOD
Department of Mechanical and Aerospace Engineering, Arizona State University, Tempe, AZ 85287, U.S.A.

(*Received* 5 *July* 1988 *and in final form* 7 *February* 1989)

Abstract—A numerical analysis of developing laminar flow between vertical parallel plates is presented for combined heat and mass transfer natural convection with uniform wall temperature and concentration boundary conditions. For long channels (low Rayleigh numbers) the numerical solutions approach the fully developed flow analytical solution. At higher Rayleigh numbers, the present results are compared with the available experimental data and numerical solutions for natural convection heat transfer in channels, and with external combined heat and mass transfer free convection similarity solutions for a single plate. At intermediate Rayleigh numbers, the parallel plate heat and mass transfer is higher than that for a single plate, similar to previous results for heat transfer only.

INTRODUCTION

IN THIS paper, numerical results are reported for developing laminar natural convection flow in a vertical parallel plate channel open to the ambient at the top and bottom. The fluid motion is generated by the combined buoyancy of temperature and concentration differences within the channel relative to the fluid surrounding the channel.

Each wall may be individually maintained at a uniform temperature and concentration (*UWT*/*C*). Two specific combinations of boundary conditions are examined: symmetric *UWT*/*C*, and a *UWT*/*C* wall opposed by a zero heat and mass flux wall (i.e. insulated). Rayleigh numbers in the range from fully developed flow up to the limit for back flow at the channel exit are investigated. The majority of the results are for a Prandtl number of 0.7 and Schmidt numbers between 0.2 and 5.0.

Previous work

Combined heat and mass transfer natural convection has previously been studied mostly for external flows. Gebhart and Pera [1] obtained similarity solutions for flow over a vertical plate with uniform temperature and concentration, and for point source or plume flows. Chen and Yuh [2] also obtained similarity solutions for inclined plates with either uniform heat and mass flux or uniform temperature and concentration boundary conditions.

Analytical solutions for fully developed flow for the present problem are given in ref. [3]. Results for developing flow with uniform heat and mass flux boundary conditions were previously reported in ref. [4]. Lee *et al.* [5] considered a vertical channel flow for very specific conditions in which mass transfer from one wall resulted in a downward flow while heat transfer on the other wall resulted in an opposing, upward flow. Here we consider only flows which are entirely rising or falling, even though the buoyancy due to mass transfer may be opposed to the buoyancy due to heat transfer.

Developing natural convection heat transfer between vertical parallel plates has been considered more extensively. Symmetric uniform wall temperature conditions were investigated experimentally by Elenbaas [6] and numerically by Bodoia and Osterle [7] and Aihara [8]. Aung *et al.* [9] considered asymmetric uniform heat flux and uniform wall temperature boundary conditions as did Miyatake and Fujii [10, 11] and Miyatake *et al.* [12]. Miyatake and Fujii [13], Sparrow *et al.* [14] and Sparrow and Azevedo [15] considered a uniform temperature wall bounded by an insulated wall. Wirtz and Stutzman [16] and Applebaum [17] reported experimental results for uniform heat flux parallel plates in air for symmetric and asymmetric heating, respectively.

All of the previous studies of developing natural convection heat transfer between parallel plates have found a 5–20% increase in heat transfer when compared to the corresponding single, external plate. The present results are similarly compared with the corresponding combined heat and mass transfer single plate results.

NOMENCLATURE

b	channel width [m]
C	species mass fraction
D	species diffusivity [$m^2 s^{-1}$]
g	gravitational acceleration [$m s^{-2}$]
Gr	channel Grashof number based on b and l
h	convective heat transfer coefficient, $q_1/(T_1-T_0)$
h_m	convective mass transfer coefficient, $m_1/(C_1-C_0)$
k	thermal diffusivity [$W m^{-1} K^{-1}$]
l	channel length [m]
L	non-dimensional channel length, l/Gr
Le	Lewis number, $Sc/Pr = \alpha/D$
m	mass flux [$kg s^{-1} m^{-2}$]
N	buoyancy due to mass transfer parameter
Nu	Nusselt number, hb/k
p	pressure [Pa]
p'	local hydrostatic pressure (0 at $x = 0$) [Pa]
P	dimensionless pressure
Pr	Prandtl number, ν/α
q	heat flux [$W m^{-2}$]
Q	non-dimensional volume flow rate per unit depth
Ra	Rayleigh number, $Gr\,Pr$
Sc	Schmidt number, ν/D
Sh	Sherwood number, $h_m b/D$
T	fluid temperature [K]
u	velocity in the x-direction [$m s^{-1}$]
v	velocity in the y-direction [$m s^{-1}$]
x	distance along the channel [m]
y	distance across the channel [m]
Z	fully developed flow scaling parameter.

Greek symbols

α	thermal diffusivity [$m^2 s^{-1}$]
β	volumetric coefficient of thermal expansion
β^*	volumetric coefficient of concentration expansion
θ	non-dimensional fluid temperature
ν	kinematic viscosity [$m^2 s^{-1}$]
ρ	fluid density [$kg m^{-3}$].

Subscripts

0	channel inlet, reference
1	reference wall at $y = 0$
2	wall at $y = b$
b	based on dimension b
c	concentration
t	temperature
x	at a distance x from channel entrance.

ANALYSIS

Consider a duct comprised of two vertical parallel plates of length l spaced a distance b apart as shown in Fig. 1. As a result of both heat and mass transfer at the walls, the fluid in the duct is at a higher temperature and concentration than the surrounding fluid. The resultant density difference in the presence of a gravitational field causes the fluid in the channel to rise.

Many processes in air occur at low concentration, small temperature differences and over distances of small vertical extent relative to the atmospheric scale height (≈ 8 km). Under these conditions it is reasonable to neglect the normal component of velocity due to mass transfer at the walls, viscous dissipation and pressure work. If the molecular weight of the diffusing species is not too different from air, then diffusion of mass due to temperature gradients (thermal diffusion) and diffusion of energy due to concentration gradients (diffusion-thermo) may also be neglected.

When the governing equations are nondimensionalized, the group $(b/l)^2$ occurs multiplying the axial diffusion terms $(\partial^2/\partial X^2)$. For $(b/l)^2 \ll 1$, the axial diffusion terms are negligible in comparison to the convection and transverse diffusion terms, and a parabolic form of the governing equations results. A linear equation of state and the Boussinesq approximation (see Gebhart and Pera [1]) allow the constant

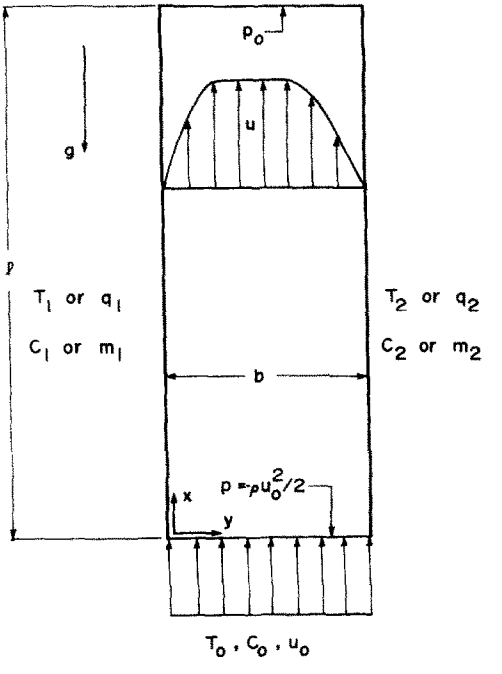

FIG. 1. Geometry and boundary conditions.

property, incompressible form to be retained. The non-dimensional equations describing steady, two-dimensional laminar conservation of mass, momentum, energy and species concentration are

$$\frac{\partial U}{\partial X}+\frac{\partial V}{\partial Y}=0 \tag{1}$$

$$U\frac{\partial U}{\partial X}+V\frac{\partial U}{\partial Y}=-\frac{\mathrm{d}P}{\mathrm{d}X}+\frac{\partial^2 U}{\partial Y^2}+\theta+NC \tag{2}$$

$$U\frac{\partial \theta}{\partial X}+V\frac{\partial \theta}{\partial Y}=\frac{1}{Pr}\frac{\partial^2 \theta}{\partial Y^2} \tag{3}$$

$$U\frac{\partial C}{\partial X}+V\frac{\partial C}{\partial Y}=\frac{1}{Sc}\frac{\partial^2 C}{\partial Y^2} \tag{4}$$

where

$$X=\frac{x}{lGr},\quad Y=\frac{y}{b}$$

$$U=\frac{b^2 u}{lv\,Gr},\quad V=\frac{bv}{v}$$

$$P=\frac{(p-p')b^4}{\rho l^2 v^2 Gr^2}$$

$$\theta=\frac{T-T_0}{T_1-T_0},\quad C=\frac{C-C_0}{C_1-C_0}$$

$$Gr=\frac{g\beta(T_1-T_0)b^4}{lv^2},\quad N=\frac{\beta^*(C_1-C_0)}{\beta(T_1-T_0)}.$$

The non-dimensional boundary conditions are

$$U(X,0)=U(X,1)=V(X,0)=V(X,1)=0$$

$$U(0,Y)=Q$$

$$\theta(0,Y)=C(0,Y)=0$$

$$\theta(X,0)=1,\quad \theta(X,1)=\frac{T_2-T_0}{T_1-T_0}=r_t$$

$$C(X,0)=1,\quad C(X,1)=\frac{C_2-C_0}{C_1-C_0}=r_c.$$

A uniform inlet velocity profile was used based on the results of Aihara [8]. For a uniform inlet velocity profile, the inlet pressure drop required to accelerate the fluid from rest to the inlet is

$$P(0)=-Q^2/2.$$

Including this inlet pressure drop has a small but non-negligible effect on the channel induced flow rate and heat and mass transfer at higher Rayleigh numbers. At the channel exit, the flow becomes a free jet and expands to the local hydrostatic pressure at that elevation

$$P(L)=0.$$

Since the flow is internal and the local pressure gradient is unknown, the additional constraint of a global conservation of mass equation is required. At any cross-section in the channel, the mass flow rate must be the same

$$Q=\frac{\bar{u}b^2}{lv\,Gr}=\int_0^1 U\,\mathrm{d}Y. \tag{5}$$

The above set of equations and boundary conditions are solved by a second-order accurate, Crank–Nicholson finite difference method using iteration for the convective nonlinearity and coupling between equations. A few of the unique aspects of the implementation for this problem are discussed below.

The pressure–velocity coupling is used to generate the proper pressure gradient in the following way. The finite difference form of the momentum equation is solved (algebraically) for the currently unknown velocity at a general node. This is then integrated (algebraically) across the channel using Simpson's rule and the result is set equal to the prescribed mass flow rate, Q. The pressure gradient term is then isolated and evaluated (computationally) from this form. More sophisticated methods which simultaneously satisfy the momentum and global conservation of mass equations are not as useful in this case because the local buoyancy force in the momentum equation is not known beforehand and the equations must be solved iteratively. The present technique enforces global conservation of mass at every iteration and typically gives a relative mass flow error of 10^{-5}.

For a channel flow, a zero normal velocity V should be imposed on both walls (or the wall and the centerline for a symmetric case). Since the y-momentum equation has been dropped in the parabolic formulation and the conservation of mass equation is first order in y, only one boundary condition may properly be imposed on V. Bodoia and Osterle [7] simply integrate from the wall out to the centerline without imposing a condition at the centerline as is done in external boundary layer flows. Aung *et al.* [9] impose $V=0$ on each wall and integrate out to within one node of either side of the centerline and then interpolate the centerline node value, regardless of the asymmetry of the problem. In the present work, $V=0$ is imposed on each wall and two solutions are obtained by integrating from one wall to the other and then in the reverse order. The two solutions are then added together, each weighted by the distance from the wall from which it was calculated, to obtain the final V field. This method gives a solution that approximately satisfies the local conservation of mass equation for all ranges of asymmetry without concentrating at a single node the error associated with imposing two boundary conditions.

Grid refinement tests were performed to insure that the present results are independent of grid size. A uniform grid in the Y-direction was used with 21 grid points at low Ra and up to 81 grid points at high Ra. The non-uniform X grid was stretched 4% per step up to a maximum of $L/100$ resulting in 200–1000 axial grid points. The iteration at a particular X was considered converged when the relative change in velocity U at each point was less than 10^{-5} for two consecutive iterations. The changes in P, T and C were

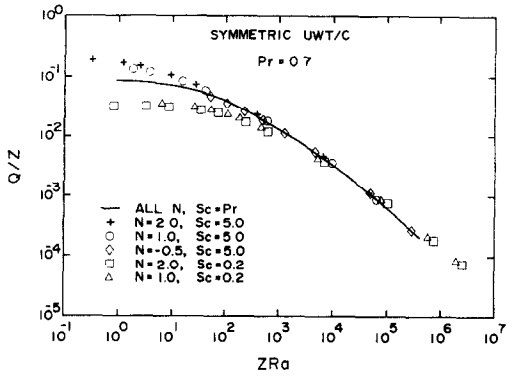

FIG. 2. Induced flow rate for symmetric *UWT/C*.

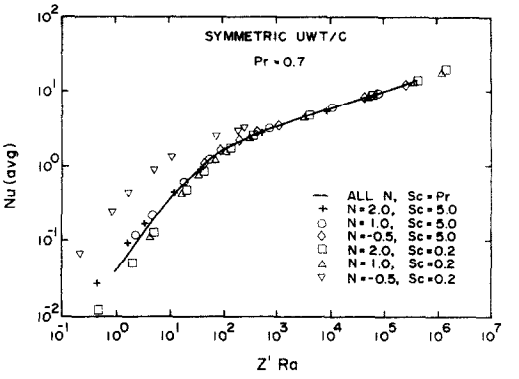

FIG. 3. Average Nusselt number for symmetric *UWT/C*.

then usually less than 10^{-5}. The overall momentum, energy and species concentration balances were all within 1%

RESULTS

Symmetric UWT/C

For *UWT/C* fully developed flow (see ref. [3]), the non-dimensional induced flow rate is independent of *Pr*, *Sc* and *Ra*. When the present developing flow case is plotted in terms of the fully developed flow parameters $Q/(1+N)$ vs $(1+N)Ra$, all of the results converge to the fully developed value for $(1+N)Ra < 2$, but each combination of N and Sc behaves differently at higher *Ra*. The developing *UWT/C* flow has a net addition of heat and mass to the flow stream that is similar to the fully developed uniform heat and mass flux (*UH/MF*) flow but which is absent in the fully developed *UWT/C* flow. When the flow rate for the present case is plotted in terms of the fully developed *UH/MF* scaling parameter

$$Z = \{1+r_h+N(1+r_m)/Le\}/2 \qquad (6)$$

(with r_h and r_m replaced by $r_t = r_c = 1$ for symmetric *UWT/C*), Fig. 2 results. For $Z\,Ra > 10^3$, all of the results converge to a nearly universal curve. As for the *UH/MF* developing flow case (see ref. [4]), the $Sc = 0.2$ results fall slightly above the other results.

The maximum $(1+N)Ra$ that could be achieved was 4×10^5 for $Sc = Pr$. At this value, the velocity profile was very peaked on either side with a maximum velocity approximately three times the average velocity and near zero velocity at the centerline (see Fig. 6). At higher $(1+N)Ra$ backflow at the exit would occur; thus, this is the $(1+N)Ra$ limit for the present parabolic model. This maximum $(1+N)Ra$ was influenced only slightly by N and Sc for N positive. For N negative and small Sc, the $(1+N)Ra$ for backflow was reduced significantly as the negatively buoyant species diffuses quickly to the center of the channel, reducing the velocity there. For $N = -0.5$ and $Sc = 0.2$, backflow at the exit occurred at $(1+N)Ra = 2\times10^3$. At higher values of *Ra*, backflow at the exit will eventually destroy the pressure gradient in the channel. The present case should then asymptotically approach the single-plate results of Gebhart and Pera [1].

The average Nusselt number calculated for the developing flow is within 5% of the fully developed solution for $(1+N)Ra < 2$. When *Nu* is plotted against *Z Ra*, good correlation is obtained at high *Ra*, but better results are obtained if the square root of *Le* is substituted in *Z*

$$Z' = \{1+r_t+N(1+r_c)/\sqrt{(Le)}\}/2. \qquad (7)$$

When Z' is used, as shown in Fig. 3, all of the average *Nu* results for $Z'\,Ra > 10^3$ converge to

$$Nu = 0.705(Z'\,Ra)^{0.230}. \qquad (8)$$

Equation (8) predicts between 13 and 15% higher *Nu* at $Z'\,Ra = 10^4$ and between 7 and 9% higher *Nu* at $Z'\,Ra = 10^5$ than the single plate results of Gebhart and Pera [1]. At $Z'\,Ra = 6.6\times10^6$, which is above the backflow limit of the present solution method, equation (8) predicts the same *Nu* as the $Sc = Pr$ results of Gebhart and Pera [1]. The present results for $Sc = Pr$ compare very closely with Aihara's [8] *UWT* heat transfer results using a uniform inlet velocity profile and inlet pressure drop.

When $Z'\,Ra$ is multiplied by Le^2, equation (8) may be used to predict the Sherwood number for $Le^2\,Z'\,Ra > 10^3$ for most of the results. As shown in Fig. 4, the $Sc = 5$ results fall below the other results and are well correlated by

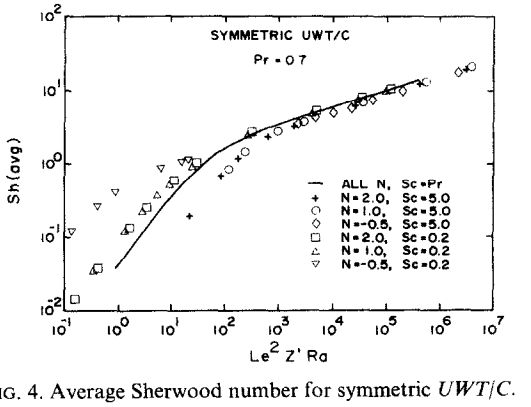

FIG. 4. Average Sherwood number for symmetric *UWT/C*.

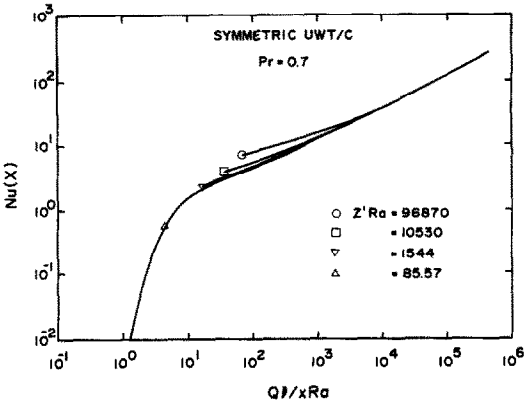

FIG. 5. Local Nusselt number for symmetric *UWT/C*.

$$Sh = 0.559(Le^2 Z' Ra)^{0.239} \quad (9)$$

for $Le^2 Z' Ra > 10^3$. Equation (9) predicts from 9% ($N = 2$) to 14% ($N = -0.5$) higher Sh at $Le^2 Z' Ra = 10^4$ and 6% ($N = 2$) to 11% ($N = -0.5$) higher Sh at $Le^2 Z' Ra = 10^5$ than the single plate $Sc = 5$ results of Gebhart and Pera [1].

Local results. The parameter group $Q(l/x)Ra$ is a local Graetz number for the present problem suggested by the fully developed flow solution. In Fig. 5, the symbols mark the exit of the duct ($x/l = 1$) and identify the overall Rayleigh number ($Z' Ra$) for a particular local Nusselt number curve. A figure similar to Fig. 5 represents the local Sherwood number when the abscissa is multiplied by the Lewis number.

At low $Z' Ra$, $Nu(x)$ smoothly changes from a constant slope near the inlet toward a rapidly increasing slope near the exit. At higher $Z' Ra$, $Nu(x)$ follows the same slope near the inlet, but then breaks away from the lower $Z' Ra$ results and follows a lower slope. This change in slope occurs closer to the inlet for higher $Z' Ra$.

The local Nusselt numbers exhibit three characteristics.

(1) Fully developed flow—$Nu(x)$ tends toward zero; occurs at low $Q(l/x)Ra$ for low $Z' Ra$.

(2) Forced convection type behavior—$Nu(x)$ follows a 1/2 slope; occurs near the inlet (high $Q(l/x)Ra$) for all flows over a small region (note the log scale).

(3) Single, external plate type behavior—$Nu(x)$ follows a 1/4 slope; occurs at higher $Q(l/x)Ra$ for higher $Z' Ra$.

These characteristics are also observed in the development of the U velocity profiles in Fig. 6. At higher Rayleigh numbers, the buoyancy due to heat and mass transfer at the walls is strong enough to cause entrainment of the core flow into the wall region. The local Nusselt number in Fig. 5 begins to follow a 1/4 slope at the point where two symmetric peaks in the U velocity profile first occur in Fig. 6. The local V velocity is then from the centerline toward each wall and the channel starts to behave as an external flow on two single, independent plates. Note that the average results in Figs. 3 and 4 have a constant slope (near 1/4) for $Z' Ra > 10^3$, similar to a single plate.

Insulated UWT/C

The case of one wall held at *UWT/C* while the opposing wall has zero heat and mass flux is referred to as the insulated *UWT/C* case. At low Ra, this case has the same fully developed flow solution as the symmetric *UWT/C* case because the insulated wall attains T_1 and C_1 by diffusion across the channel. At high Ra, this case behaves like an asymmetric *UWT/C* case with $r_t = r_c = 0$ because the fluid at the insulated wall is still at T_0 and C_0. The insulated case was chosen because it has more practical application than the asymmetric *UWT/C* configuration and allows comparison with some interesting experimental heat transfer and flow visualization results.

The maximum $(1+N)Ra$ that could be calculated before backflow (separation) occurred on the insulated wall was 1.2×10^3 for $Sc = Pr = 0.7$. Because this flow never reaches the high Ra developing region and has mixed-type boundary conditions, the scaling used for symmetric *UWT/C* (Z') is not useful for this case. The induced flow rate is shown in Fig. 7. The value of $(1+N)Ra$ at which the flow rate becomes fully developed varies with both N and Sc.

The average Nusselt number results are shown in Fig. 8. All of the results are within 5% of the symmetric *UWT/C* fully developed flow solution for $(1+N)Ra < 2$. As shown in Fig. 9, the same is true for the average Sherwood number for $Le(1+N)Ra < 2$. Since the results in Figs. 8 and 9 are unscaled with respect to $N/\sqrt{(Le)}$, some trends are evident in the developing flow region that may not be noticeable in the previous results. For $N > 0$ (aiding buoyancy), $Sc > Pr$ tends to decrease Nu and increase Sh relative to $Sc = Pr$ while for $Sc < Pr$ the reverse is true. However, $N < 0$ (opposing buoyancy) tends to decrease both Nu and Sh for all Sc. This behavior was also noted for external flows by Gebhart and Pera [1] and Chen and Yuh [2].

Sparrow *et al.* [14] report experimental and numerical results for natural convection heat transfer between a *UWT* plate and an insulated plate in water. The present method was used to calculate Nu for $Pr = 5.0$ as shown in Fig. 10. Also shown are the numerical results (using a uniform inlet velocity profile and an inlet pressure drop) and the least squares fit of the experimental data (estimated error of $\pm 2\%$) given by Sparrow *et al.* [14]. The agreement is excellent between the two numerical results, and the present calculation underpredicts the experimental data by about 5% for Ra between 200 and 2000.

Sparrow *et al.* [14] also report flow visualization results from the experiments. They observed backflow at the exit on the unheated wall for Ra between 1600 and 2130 when b/l was varied between 0.0437 and 0.0656. Using the present calculation method, backflow on the unheated wall occurred at $Ra = 2424$. Sparrow *et al.* [14] and Sparrow and Azevedo [15]

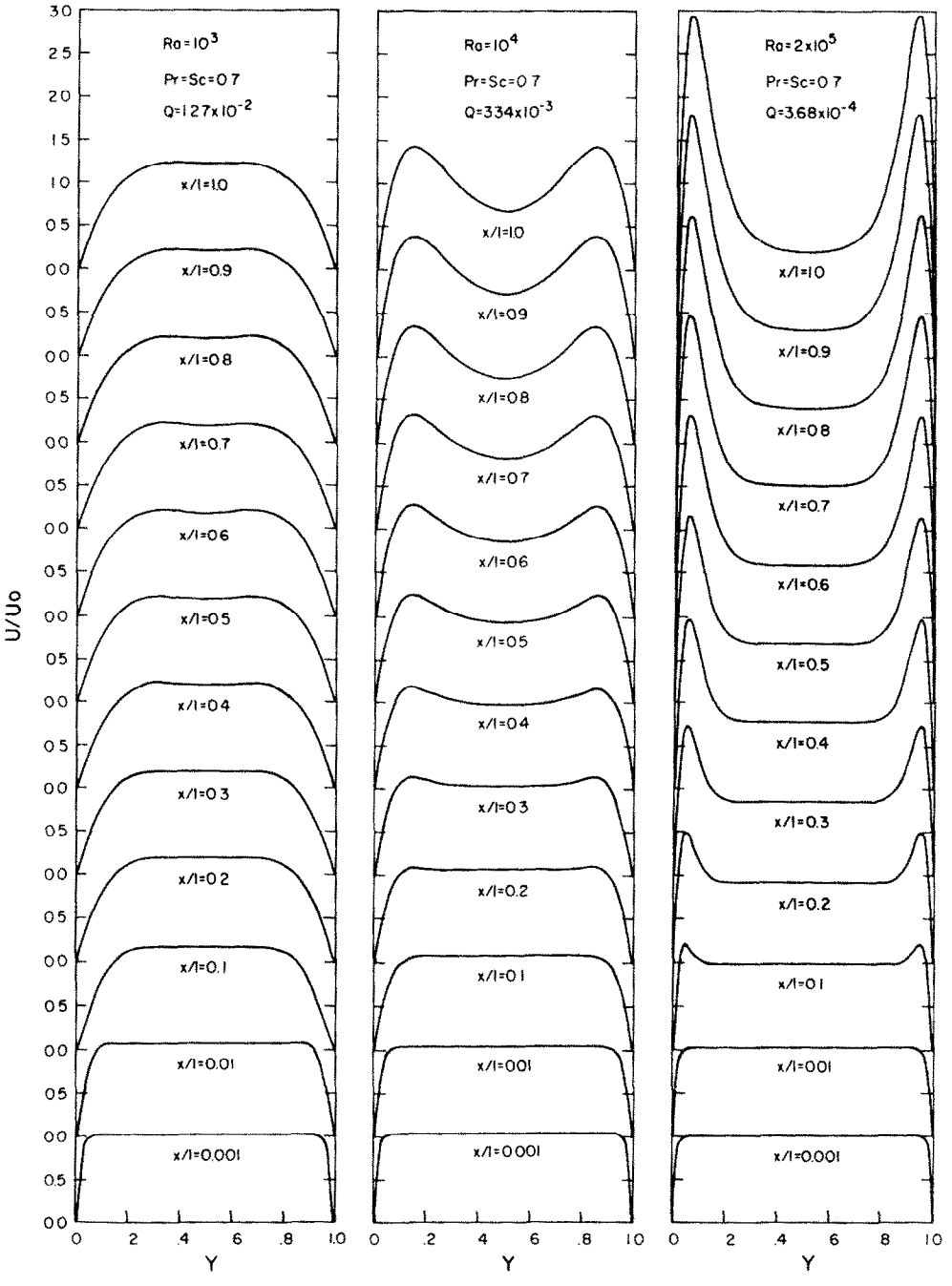

FIG. 6. Development of U velocity profiles.

obtained numerical solutions up to $Ra = 8 \times 10^4$ and 10^8, respectively, using a model which 'did not account for vertical downflow', but no explanation of the method was given in either of the papers or the references cited. The present method is able to predict the occurrence of backflow at the channel exit.

Local results. The local Nusselt number for $Sc = Pr = 0.7$ is shown in Fig. 11. The same general characteristics as Fig. 5 are observed. The insulated UWT/C Nusselt number is higher than the symmetric results for $Q(l/x)Ra < 10$. At the highest $(1+N)Ra$ of 1246, the local Nu begins to rise above the lower Rayleigh number results, similar to the symmetric UWT/C case at Z' $Ra = 1000$ when the peaks in the velocity profile first form.

CONCLUSIONS

A numerical solution of the governing equations for natural convection between vertical parallel plates has been presented for buoyancy due to combined heat and mass transfer. The solution has been verified

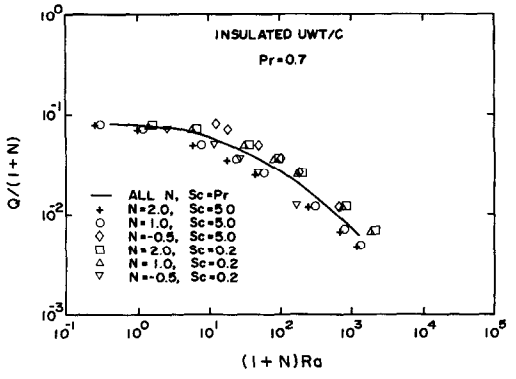

FIG. 7. Induced flow rate for insulated *UWT/C*.

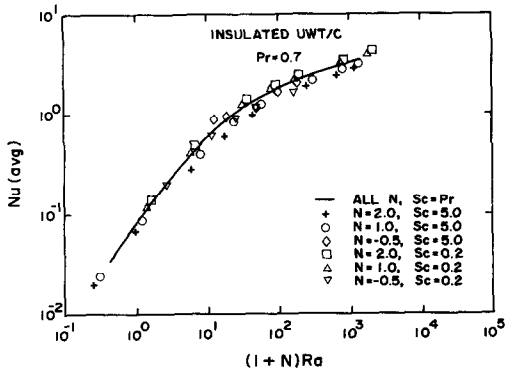

FIG. 8. Average Nusselt number for insulated *UWT/C*.

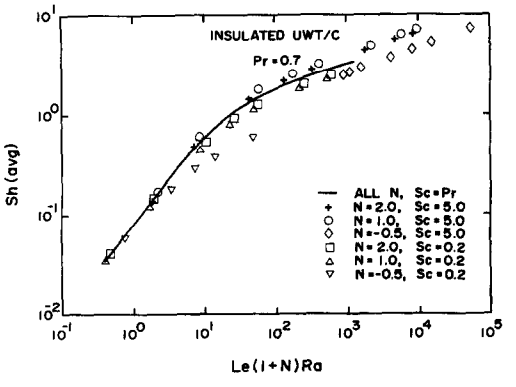

FIG. 9. Average Sherwood number for insulated *UWT/C*.

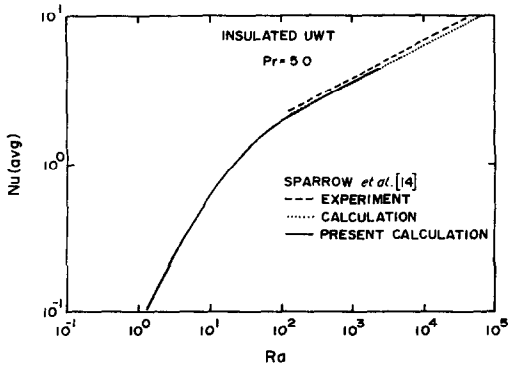

FIG. 10. Comparison of average Nusselt number with experimental and numerical results of Sparrow *et al.* [14].

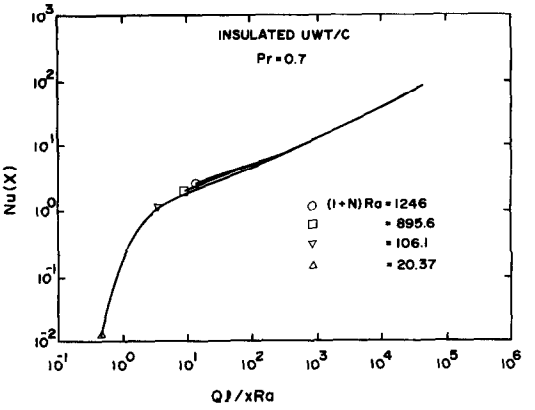

FIG. 11. Local Nusselt number for insulated *UWT/C*.

by comparison of the present results with available experimental heat transfer data. The results cover a wide range of Rayleigh numbers from fully developed flow up to backflow at the exit for both aiding and opposing buoyancy due to mass transfer (N).

The maximum Rayleigh number that can be calculated using the present parabolic method corresponds to the first occurrence of backflow at the channel exit. For $Sc = Pr$ this occurs at $(1+N)Ra = 4 \times 10^5$ for the symmetric uniform wall temperature and concentration case and $(1+N)Ra = 1.2 \times 10^3$ for the insulated uniform wall temperature and concentration case. The maximum Rayleigh number is weakly influenced by Sc and N for $N > 0$ and strongly influenced by $N < 0$.

The present method of treating the conservation of mass equation and boundary conditions is reasonably well verified by comparison of the calculated Rayleigh number for backflow with the experiment of Sparrow *et al.* [14] for the insulated uniform wall temperature case.

The present developing flow calculations approach the fully developed flow solution at low Rayleigh numbers. The fully developed flow solution may be used for $(1+N)Ra < 2$. A modified form of the uniform heat and mass flux fully developed flow scaling, Z', is useful for correlating the high Rayleigh number results for the symmetric uniform wall temperature and concentration case.

At high Rayleigh numbers, the symmetric case exhibits a constant slope Nusselt and Sherwood number (in log coordinates) that is similar to but above a single, external plate. The formation of two separate symmetric peaks in the velocity profile corresponds to the constant slope region in the average results or a change in slope in the local results. Near the inlet, all of the results behave similar to a forced convection developing flow with a uniform inlet velocity profile.

When the proper inlet pressure is specified, the local heat and mass transfer away from the entrance approach the corresponding single plate values within a few percent at high Rayleigh numbers. The average values are 5–15% higher than the single-plate case due

to the forced-convection type contribution near the entrance. Previous studies of natural convection heat transfer between parallel plates have found a similar advantage over a single plate. When properly scaled, the combined heat and mass transfer aspect of the present problem does not significantly change this conclusion.

Acknowledgments—This work was supported by the U.S. Department of Energy. An American Public Power Association Energy Services Scholarship for the first author while attending Arizona State University is also gratefully acknowledged.

REFERENCES

1. B. Gebhart and L. Pera, The nature of vertical natural convection flows resulting from the combined buoyancy effect of thermal and mass diffusion, *Int. J. Heat Mass Transfer* **14**, 2025–2050 (1971).
2. T. S. Chen and C. F. Yuh, Combined heat and mass transfer in natural convection on inclined surfaces, *Numer. Heat Transfer* **2**, 233–250 (1979).
3. D. J. Nelson and B. D. Wood, Fully developed combined heat and mass transfer natural convection between parallel plates with asymmetric boundary conditions, *Int. J. Heat Mass Transfer* **32**, 1789–1792 (1989).
4. D. J. Nelson and B. D. Wood, Combined heat and mass transfer natural convection between vertical parallel plates with uniform flux boundary conditions. *Heat Transfer 1986*, Vol. 4, pp. 1587–1592 (1986).
5. T. S. Lee, P. G. Parikh, A. Acrivos and D. Bershader, Natural convection in a vertical channel with opposing buoyancy forces, *Int. J. Heat Mass Transfer* **25**, 499–511 (1982).
6. W. Elenbaas, Heat dissipation of parallel plates by free convection, *Physica* **9**, 1–28 (1942).
7. J. R. Bodoia and J. F. Osterle, The development of free convection between heated vertical plates, *J. Heat Transfer* **84**, 40–44 (1962).
8. T. Aihara, Effects of inlet boundary conditions on numerical solutions of free convection between vertical parallel plates, *Rep. Inst. High Speed Mech., Tohoku Univ.* **28**, 1–27 (1973).
9. W. Aung, L. S. Fletcher and V. Sernas, Developing laminar free convection between vertical flat plates with asymmetric heating, *Int. J. Heat Mass Transfer* **15**, 2293–2308 (1972).
10. O. Miyatake and T. Fujii, Natural convection heat transfer between vertical parallel plates at unequal uniform temperatures, *Heat Transfer—Jap. Res.* **2**, 79–88 (1973).
11. O. Miyatake and T. Fujii, Natural convective heat transfer between vertical parallel plates with unequal heat fluxes, *Heat Transfer—Jap. Res.* **3**, 29–33 (1974).
12. O. Miyatake, T. Fujii, M. Fujii and H. Tanaka, Natural convective heat transfer between vertical parallel plates—one plate with a uniform heat flux and the other thermally insulated, *Heat Transfer—Jap. Res.* **2**, 25–33 (1973).
13. O. Miyatake and T. Fujii, Free convective heat transfer between vertical parallel plates—one plate isothermally heated and the other thermally insulated, *Heat Transfer—Jap. Res.* **1**, 30–38 (1972).
14. E. M. Sparrow, G. M. Chrysler and L. F. Azevedo, Observed flow reversals and measured-predicted Nusselt numbers for natural convection in a one-sided heated vertical channel, *J. Heat Transfer* **106**, 325–332 (1984).
15. E. M. Sparrow and L. F. A. Azevedo, Vertical-channel natural convection spanning between the fully-developed limit and the single-plate boundary-layer limit, *Int. J. Heat Mass Transfer* **28**, 1847–1857 (1985).
16. R. A. Wirtz and R. J. Stutzman, Experiments on free convection between vertical plates with symmetric heating, *J. Heat Transfer* **104**, 501–507 (1982).
17. M. A. Applebaum, Investigation of buoyancy induced convective heat transfer in an inclined parallel wall channel, M.S. Thesis, Department of Mechanical and Aerospace Engineering, Arizona State University (1984).

CONVECTION NATURELLE COMBINEE DE CHALEUR ET DE MASSE ENTRE DES PLAQUES PARALLELES VERTICALES

Résumé—Une analyse numérique du développement de l'écoulement laminaire entre deux plaques verticales parallèles concerne la convection naturelle de chaleur et de masse avec des conditions aux limites de température et de concentration uniformes sur les parois. Pour les canaux longs (faible nombre de Rayleigh) les solutions numériques s'approchent de la solution analytique de l'écoulement pleinement établi. Aux grands nombres de Rayleigh, les résultats obtenus sont comparés avec les données expérimentales disponibles et les solutions numériques pour la convection thermique dans les canaux, et avec les solutions affines de convection naturelle combinée de chaleur et de masse sur une plaque unique. Aux nombres de Rayleigh intermédiaires, le transfert de chaleur et de masse pour plaques parallèles est plus élevé que pour une seule plaque, de la même façon que dans des résultats connus pour le transfert de chaleur seul.

GEKOPPELTE THERMISCHE UND KONZENTRATIONSGETRIEBENE NATÜRLICHE KONVEKTION ZWISCHEN SENKRECHTEN, PARALLELEN PLATTEN

Zusammenfassung—Es wird eine numerische Untersuchung der sich entwickelnden laminaren Strömung zwischen senkrechten, parallelen Platten für temperatur- und konzentrationsgetriebene natürliche Konvektion vorgestellt. Temperatur und Konzentration an der Wand sind dabei konstant. Für lange Kanäle (kleine Rayleigh-Zahl) nähern sich die numerischen Lösungen der analytischen Lösung für voll ausgebildete Strömung an. Für höhere Rayleigh-Zahlen werden die berechneten Ergebnisse mit verfügbaren experimentellen Daten und mit numerischen Lösungen für den Wärmetransport bei natürlicher Konvektion in Kanälen sowie mit Ähnlichkeitslösungen für die mit Wärme- und Stofftransport gekoppelte freie Konvektion an einer einzelnen Platte verglichen. Für mittlere Rayleigh-Zahlen ist der Wärme- und Stofftransport bei parallelen Platten größer als der bei einer einzelnen Platte, ähnlich wie bei früheren Ergebnissen für reinen Wärmetransport.

СЛОЖНЫЙ ТЕПЛО- И МАССОПЕРЕНОС ПРИ ЕСТЕСТВЕННОЙ КОНВЕКЦИИ МЕЖДУ ВЕРТИКАЛЬНЫМИ ПАРАЛЛЕЛЬНЫМИ ПЛАСТИНАМИ

Аннотация—Численно исследуется развитие ламинарного течения между вертикальными параллельными пластинами при сложном свободноконвективном тепло- и массопереносе для случая однородных температурнах и концентрационных граничных условий на стенках. В приближении длинного канала (малые числа Рэлея) численное решение стремится к аналитическому решению, описывающему полностью развитое течение. При более высоких числах Рэлея результаты сравниваются с имеющимися экспериментальными данными и численными решениями для свободноконвективного теплопереноса в каналах, а также с автомодельными решениями уравнений сложного тепло- и массопереноса при естественной конвекции для одной пластины. При промежуточных значениях числа Рэлея тепло- и массоперенос для параллельных пластин является более интенсивным, чем для одной пластины. Это обстоятельство согласуется с ранее найденными результатами, относящимися только к теплопереносу.